Insulating State and Breakdown of Fermi Liquid Description in Molecular-Scale Single-Crystalline Wires of Gold

U. Chandni,[†] Paromita Kundu,[‡] Abhishek K. Singh,[‡] N. Ravishankar,[‡,*] and Arindam Ghosh[†,*]

[†]Department of Physics and [‡]Materials Research Centre, Indian Institute of Science, Bangalore 560 012, India

ABSTRACT Electrical transport measurements on ultrathin single-crystalline Au nanowires, synthesized *via* a wet chemical route, show an unexpected insulating behavior. The linear response electrical resistance exhibits a power-law dependence on temperature. In addition, the variation of current over a wide range of temperature and voltage obeys a universal scaling relation that provides compelling evidence for a non-Fermi liquid behavior. Our results demonstrate that the quantum ground state in ultrathin nanowires of simple metallic systems can be radically different from their bulk counterparts and can be described in terms of a Tomonaga–Luttinger liquid (TLL), in the presence of remarkably strong electron–electron interactions.

KEYWORDS: Luttinger liquid · one-dimensional transport · gold nanowires · oriented attachment process · Fermi liquid

The electrical properties of metallic nanostructures, which find a range of applications in nanoscale devices to circuits, are generally understood in terms of the Fermi liquid (FL) theory.[1−4] In the macroscopic scale, electron interaction effects in simple metals, such as gold, silver, *etc.*, are weak and hence prohibit collective non-Fermi liquid (NFL) behavior.[5] However, one-dimensional (1D) systems are special in that they are expected to contain collective excitations of a TLL[6,7] even when the interaction is infinitesimally weak.[1,2,8] Such excitations have been claimed in a variety of systems including 1D semiconductor heterostructures,[9−11] nanowires[12] and polymers,[13] charge density wave nanowires,[14] carbon nanotubes,[15−17] atomic chains,[18] *etc.* Striking phenomena like charge-spin separation,[10] zero-bias anomalies (ZBAs),[19] nonuniversal conductance quantization,[9] and unusual dependence of conductivity on temperature[12,13,15,17] are often interpreted as NFL effects in the quasi-1D regime. However, the evidence for NFL effects in metals is rather sparse owing to difficulties associated with the fabrication of stable 1D metallic structures, unavailability of protocols to synthesize such ultrathin nanostructures of high quality, and lack of placement and nondestructive contacting methods.

The prerequisite for the experimental realization of 1D systems involves confinement to channels almost as narrow as the electron Fermi wavelength, which in semiconductors is on the order of a few tens of nanometres but can be nearly 2 orders of magnitude smaller in the case of metals. Current experimental approaches for producing 1D/quasi-1D systems of metals range from nanostrips fabricated using nanolithographic edge technique,[4] polycrystalline metal wires (10 nm or greater in diameter) by template/lithographic techniques,[20] or electron-beam irradiation[21] to monatomic break junctions.[22] Experiments showing weak localization[4] and conductance quantization[22] have led to considerable interest, but they can be addressed adequately within the FL framework. In contrast, scanning tunneling microscopy studies on atomic chains of gold reported very recently[18] showed distinct NFL characteristics and constitute the only reported work in this regime to date. The recent discoveries[23−26] of simple wet chemical synthesis protocols to produce ultrathin single-crystalline Au nanowires (∼2 nm in diameter) provide a new route to probe the properties of molecular-scale metal wires. In this method, attachment of ultrafine nanoparticles (with a very narrow size distribution) in the solution phase or on substrates is facilitated by selective removal of capping agent from specific crystallographic facets and leads to the formation of long ultrafine nanowires of uniform diameter amenable to transport measurements. We present the electrical transport characteristics in these wires, which are strongly suggestive of an NFL behavior and emergence of 1D/quasi-1D TLL even in a simple metallic system.

RESULTS AND DISCUSSION

Ultrathin Au nanowires have been grown directly on insulating (Si/SiO_2) substrates. Figure 1a–c illustrates transmission electron microscopy (TEM) images of such wires

* Address correspondence to nravi@mrc.iisc.ernet.in, arindam@physics.iisc.ernet.in.

Received for review August 19, 2011 and accepted September 23, 2011.

Published online September 23, 2011
10.1021/nn2031935

grown in the solution phase, at progressively higher magnifications, showing long wires (>1 μm long) on the order of 2 nm diameter. The high-resolution TEM image of a wire segment shows the single-crystalline face-centered nature of the wires with the long axis along a ⟨111⟩ direction. In general, growth of isolated single nanowires to bunches (up to ~30) of nanowires could be achieved by tuning the growth parameters. On the Si/SiO_2 substrates, the nanowire bunches consisted of laterally stacked or fused nanowires, forming flat ribbons/strips. A symmetry-unrestricted relaxation of the nanowires (1.8 nm diameter) using density functional calculations (Supporting Information) shows relaxation in the outermost layers of the nanowires while the core atoms maintain their bulk positions (Figure 1d).

Being among the thinnest single-crystalline nanowires ever measured, the challenging aspect of device fabrication is attaching the electrical leads. First, the wires are barely resolved in a field-emission SEM, making it difficult to locate them. Prolonged exposure to electron-beam or even mild heating results in the disintegration of the wires into nanoparticles (see Supporting Information). Second, their fragile nature makes them unsuitable for standard electron-beam lithography. A special fabrication route was hence developed, where all lithography and device bonding steps were carried out at room temperature (for details, see Supporting Information). We found that the yield percentage is remarkably enhanced with this modified room temperature lithography as compared to the conventional lithographic methods (Figure 2a). In addition, static electric charges acquired during imaging and device fabrication were found to irrecoverably damage the devices. We discovered that enclosing the samples inside a custom-made humidifier, or even a dip in clean water for about 5 min, after SEM imaging but before the device bonding, resulted in a high yield (over 90%) as compared to ~12% without the humidifier (see Figure 2b). The humidifier serves as a uniform bath where the static charges accumulated during lithography/imaging can be effectively discharged without causing damage to the devices. Figure 2c,d shows typical two-probe and four-probe devices, respectively, that were fabricated using the modified method.

Electrical characterization of the nanowires consists of current−voltage ($I-V$) measurement at fixed temperatures down to ~5 K. In Figure 3a, the detailed temperature dependence of $I-V$ characteristics is shown for a two-probe device. The $I-V$ characteristics were recorded in current-limiting mode, with a maximum current of 2−20 nA, depending on the device. Within this range, the $I-V$ traces are linear at room temperature in all devices, with the resistance varying from ~50 kΩ to 20 MΩ without any systematic dependence on the nanowire number or device length

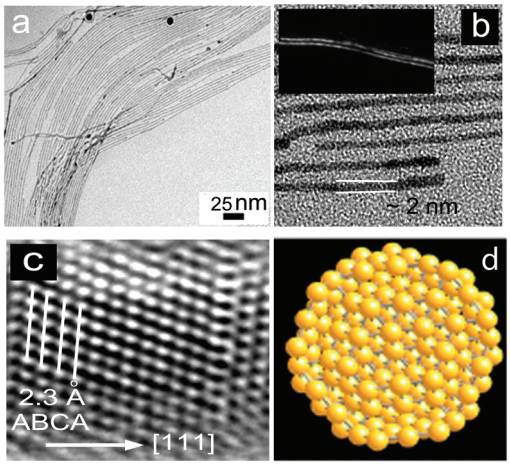

Figure 1. (a) Bright-field TEM image of an array of ultrathin Au nanowires obtained by the wet chemical route. (b) Higher magnification image recorded from a selected portion of the parallel array of wires reveals the diameter of the wire to be ~2 nm. A dark-field image of parallel wires is shown in the inset. (c) High-resolution TEM image of a wire segment revealing the interplanar spacing of 2.3 Å corresponding to {111} of fcc Au, indicating that the wires have their long axis parallel to a ⟨111⟩ direction. (d) Density functional calculations indicating the surface relaxation with the core atoms intact in their bulk positions.

(~100−300 nm). The corresponding resistivity is about 2−1000 times larger than the specific resistivity reported in thicker Au nanowires.[27,28] In the four-probe configuration, as shown in Figure 3b, the resistance of the central segment (between V_+ and V_-) of the nanowire is very similar to its own two-probe resistance, as well as that of the adjacent segments, without any systematic scaling of resistance with the length of the wire segment between voltage probes. This indicates that the electrical transport in our nanowires is different from that in conventional metallic systems where resistance is related to the length of the wire *via* a well-defined resistivity. However, the agreement between the two-probe and four-probe resistance does imply a relatively small contribution from the contacts. Hence, in the remainder of the paper, we present data and analysis from two-probe devices, with electrode configuration similar to that shown in Figure 2c. Below ~80−100 K, the $I-V$ traces become progressively nonlinear with decreasing T, irrespective of the number of nanowires in the device, resulting in an unexpected insulating behavior. The $I-V$ values were found to vary similarly with T in the four-probe devices, as well (Figure 3b), which establishes the behavior to be an intrinsic property of the nanowires, rather than due to deteriorating contact quality at low T.

Figure 3c shows the differential conductance dI/dV as a function of the source−drain bias V, which exhibits a clear ZBA in the form of a sharp dip at $V = 0$. The Altshuler−Aronov correction,[29] which treats electron−electron interactions perturbatively as in a weakly disordered metal, cannot explain the large changes in

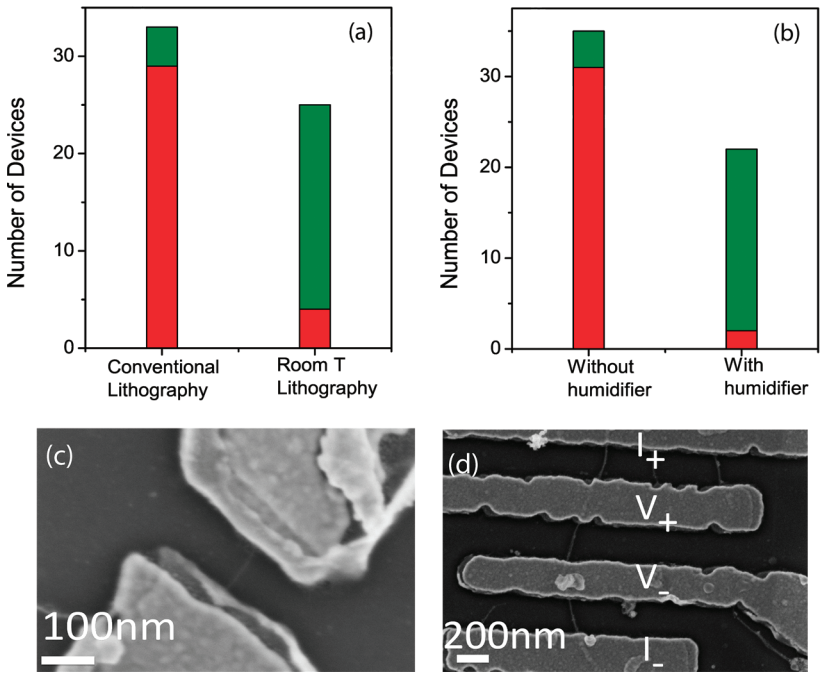

Figure 2. Device yield statistics for (a) the two different schemes of lithography and (b) for devices fabricated without and with the humidifier. Green indicates the number of successful devices, while the failed ones are indicated in red. (c) Typical two-probe device with contacts fabricated using the modified lithographic technique. (d) Four-probe device with current leads (I_+, I_-) and voltage leads (V_+, V_-).

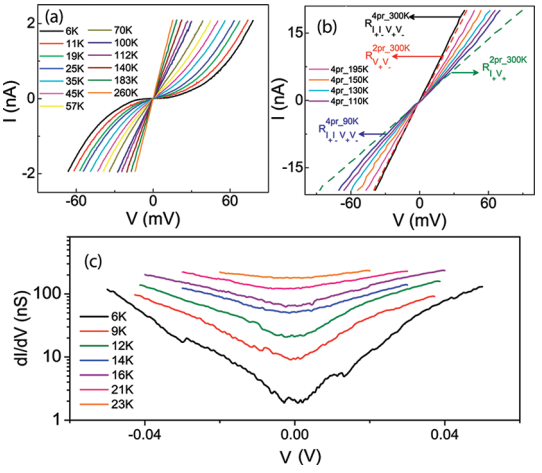

Figure 3. (a) Current−voltage ($I-V$) characteristics of a two-probe device for different temperatures. The $I-V$ values become nonlinear at low temperatures, revealing an insulating behavior that is generic to all devices. (b) $I-V$ characteristics of a four-probe device are shown for different temperatures. The red dashed line is the two-probe $I-V$ between V_+ and V_- at 300 K, with a resistance (R_{V+V-} = 2.05 MΩ) very similar to the four-probe configuration ($R_{I+I-,V+V-}$ = 1.9 MΩ), establishing low contact resistance. The two-probe $I-V$ from other parts (shown for the I_+-V_+ segment as a green dashed line) of the nanowire displays similar order of resistance magnitude, as well (R_{V+I+} = 4.3 MΩ). (c) Strong suppressions of the differential conductance (dI/dV) at the Fermi energy (E_F), for different T, indicative of a gap in the density of states at E_F. Note the change in the conductance G at E_F, $\delta G \sim G$.

the conductance that we observe ($\delta G \sim G$). Another crucial aspect of our devices was evident in the linear response regime ($eV \ll k_BT$), where we discovered that the increase in zero-bias resistance (R) followed a power law with temperature, $R \propto T^{-\alpha}$. This is true for over the entire temperature range with α varying from ~5.8 in devices with a single nanowire (within the resolution of the scanning electron micrograph) to ~1 for devices with ~30 nanowires (Figure 4a).

In 1D systems, many processes[2,12−15,30] may lead to power-law correlations in transport. However, since the current flow in most devices, including in single nanowires, occurs in multiple 1D channels, the interaction is expected to be short-ranged in nature, making a 1D Wigner crystalline state[31] unlikely. The variation of R does not fit a variable-range hopping[30] behavior in the presence of strong localization even at low T values, which in disordered 1D systems is expected to vary as $R \sim \exp[(T_0/T)^{1/2}]$ in both Mott and Efros-Shklovskii processes in 1D (see Supporting Information). This is also supported by the observation that both $R-T$ and the $I-V$ characteristics were completely unaffected by magnetic field up to 8 T. Another likely candidate is the environmental Coulomb blockade (ECB),[32] in which tunneling into a quasi-1D channel excites eigenmodes as in an LC transmision line which predicts $\alpha = 2Ze^2/h$, where Z is the line impedance.[14] The kinetic inductance for a single mode wire is calculated as $L = h/2e^2v_F$, where v_F is the Fermi velocity, and the self-capacitance is $C = 2\pi\varepsilon_0\varepsilon_r/\ln(x/r)$, where x is the distance to the leads and r is the radius of the nanowire. This gives $Z \propto (L/C)^{1/2} \approx 18.6$ kΩ gives $\alpha \approx 1.4$

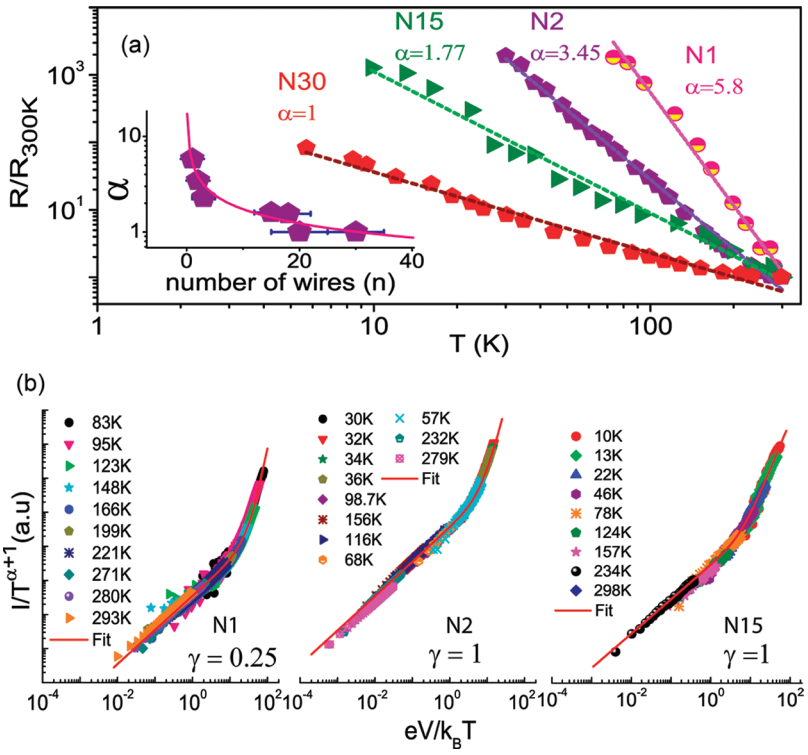

Figure 4. (a) Normalized linear response resistance (*R*) as a function of temperature for four devices with different number of wires. The numeric in the device code indicates the estimated number of nanowires in the device. In all cases, *R* increases with decreasing *T* in a power law such that $R \propto T^{-\alpha}$. The value of α is noted against the corresponding device. Inset shows the variation of temperature exponent (α) with number of nanowires (*n*). For multiple-nanowire bunches, determination of $n = W/D$, where *W* and *D* are width of the bunch and diameter of individual nanowires, respectively, is made difficult by intermittent breaks and discontinuities. The solid line is a fit to demonstrate the variation of α to be in accordance with tunneling into a TLL. (b) Scaling of *I*−*V* characteristics at different temperatures within the model of tunneling into a TLL. The scaling for three devices (with different number of nanowires) is shown. In all cases, the solid red line represents the functional form of eq 1 (see text).

that is nearly a factor of 4 lower than the experimentally observed value.

A potential transport mechanism in this context is tunneling into a TLL,[1−3] which can naturally lead to $R \sim T^{-\alpha}$, where α is determined by the interaction strength. The characteristic signature of tunneling into TLL is a power-law correlation in the nonlinear regime ($eV \gg kT$), where $I \propto V^{\alpha+1}$. The variation of $I(V,T)$ over the entire range of *V* and *T* can be combined into a single scaling relation[3,12]

$$I(V,T) = I_0 T^{\alpha+1} \sinh\left(\frac{\gamma eV}{2k_B T}\right) \left|\Gamma\left(1+\frac{\alpha}{2}+i\frac{\gamma eV}{2\pi k_B T}\right)\right|^2 \quad (1)$$

where γ signifies the fraction of the applied voltage that drops across the tunneling barrier(s).[15] Figure 4b shows the scaling of $I(V,T)$ in three devices with differing number of nanowires. With I_0 and γ as fit parameters, the *I*−*V* traces at different *T* collapse remarkably well on the theoretically expected scaling relation (eq 1), providing compelling evidence that the quasiparticle excitations in the ultrathin Au nanowires could indeed be represented by a TLL.

We now focus on the possible modes of tunneling in our devices. Two scenarios, FL (leads)−TLL (nanowire) and TLL−TLL, are schematically represented in Figure 5 for a two-probe configuration. In the case of FL−TLL[15] (Figure 5a,b), the tunneling into and out of the nanowire constitutes the dominant mechanisms. On the other hand, in the case of TLL−TLL,[12] the wire itself is disintegrated by single or multiple scatterers (Figure 5c,d), with very little contribution from the leads. A dominant FL−TLL tunneling is unlikely in our case as the two-probe and four-probe resistances (Figure 3b) indicate that the interfacial contact resistance is small compared to that of the bulk resistance, although quantum contact resistance ($h/2e^2$) is difficult to be eliminated in such small devices. The TLL−TLL picture with the resistance due to backscattering at specific locations also explains the unexpectedly large values of resistances which depend on the tunneling amplitude corresponding to the constituting barriers rather than the length or probe configurations. To further validate this, an alternate strategy of directly growing the wires between prefabricated Ti/Au contacts was employed, which showed very similar characteristics. No electron-beam lithography was carried out after the growth of the nanowires in this case. Since the nanowires grow and terminate at the Au leads, the contacts are expected to be seamlessly integrated to the nanowires, with a lower probability of external residues on the wire surface or any structural degradation of the wires during the lithography process. The *I*−*V*

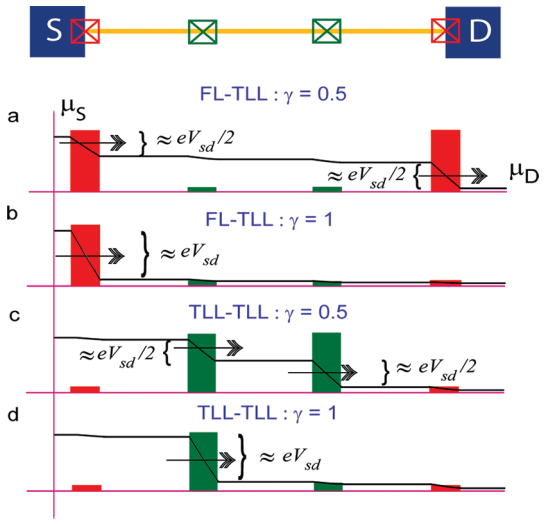

Figure 5. Schematic representation of the two possible tunneling scenarios: FL−TLL, where tunneling into and/or out of the wire gives the total impedance (a,b); and TLL−TLL, wherein the tunneling in the bulk of the wire is dominant over the contacts (c,d). The γ is a direct indicator of the number of dominant barriers present in the system: $\gamma \approx 1$ (b,d) indicates a single strong scatterer, across which most of the source voltage (*V*) drops. However, with multiple barriers of comparable strengths, $\gamma < 1$ (a,c).

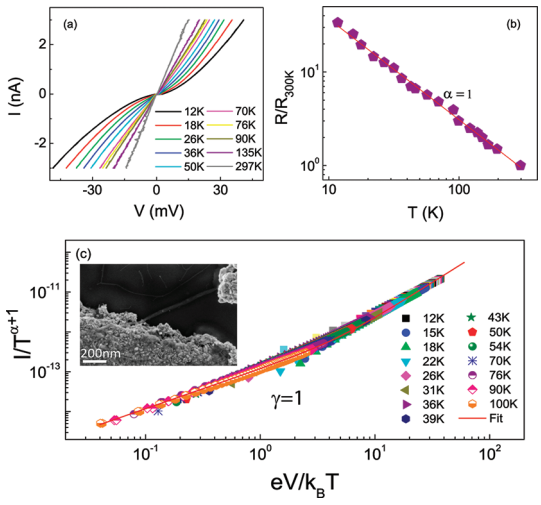

Figure 6. (a) *I*−*V* characteristics of a multiple-nanowire device grown *in situ* between two predefined Ti/Au contacts. The magnitude of linear response resistance *R* and temperature dependence of *I*−*V* characteristics bear close similarity to lithographically contacted devices. (b) Normalized *R* exhibits a power-law dependence on temperature with $\alpha \approx 1$. (c) Scaling of the *I*−*V* traces at different temperatures onto the theoretical curve defined by eq 1. Inset: SEM micrograph of the device.

characteristics, as illustrated in Figure 6a, of a typical *in situ* grown device shown as the inset in Figure 6c, bear close resemblance to the lithographically contacted devices (Figure 3 and Figure 4). In spite of the seamless contacting of the nanowires to the leads, the room temperature resistance was found to be ≈1 MΩ, which is on the same order as the lithographically contacted devices. The linear response *R* exhibits power-law dependence on *T* over the entire range, with $\alpha \approx 1$, which is reasonable for a bunched nanowire device with ∼40 nanowires (Figure 6b), confirming the TLL state. The scaling of the *I*(*V*,*T*) traces according to eq 1 with $\gamma \approx 0.8$ is shown in Figure 6c.

Strong support for the TLL−TLL tunneling was obtained from the value of γ in the scaling analysis where we found that $\gamma \approx 1$ in more than 80% of the devices. This indicates that the transport is limited by one dominant barrier across which most of the source voltage gets dropped (see Figure 5b,d). Multiple barriers of comparable impedance would, on the other hand, give $\gamma < 1$ as is indicated in Figure 5a,c. In the TLL−TLL picture, strong thickness modulations in our wires can arise not only from stacking faults or twin boundaries in the wire but also from Rayleigh−Plateau instability that has been shown to destabilize sub-10 nm metal nanowires even at room temperature.[33] Indeed, these modulations could be resolved in many of the nanowires (see Supporting Information). If the modulations are strong enough to constrict the conducting region below λ_F, strong backscattering of quasiparticles from the bulk of the TLL could lead to $R \gg h/e^2$ at low *T*. A strong scatterer of this form can then disintegrate the wire, causing tunneling from one end of a TLL to another.[17]

It is then natural to ask: Can a 2 nm Au nanowire be a 1D/quasi-1D system? As the atomistic simulations indicate, the density of states at the Fermi energy in these wires is suppressed resulting in $\lambda_F > 1.2$ nm, which indeed is close to their diameter. Whether this is from a single mode channel would require a complete band structure calculation. However, assuming the maximum observed is $\alpha \approx 5.8$, corresponding to a single mode wire in the strong backscattering regime, we get the TLL parameter[34] *g* from $\alpha = 2/g - 2$ as $g \approx 0.25$. Taking the Coulomb interaction between the electrons screened at the metallic leads,[12,32] $U \approx 4e^2 \ln(k_F L)/\pi\varepsilon_0\varepsilon_r h v_F$ (k_F, v_F, and *L* are Fermi wave vector, Fermi velocity, and sample length, respectively, and $\varepsilon_r = 1$), we get $g \approx (2/U)^{1/2} \approx 0.2$, agreeing remarkably well with the experimental observation. In the case of multiple channels with negligible interchain coupling, a description involving parallel conductors is appropriate. However, in real systems, it is more realistic to assume finite interchain coupling, with single particle tunneling between the wires.[12] In this case, $\alpha = (2/N)[(1 + NU)^{1/2} - 1]$, where *N* is the number of 1D channels, with the same v_F. The decrease in α with increasing number of wires (inset of Figure 4a) closely follows the theoretical expectation (solid line), providing additional support to the TLL picture.

CONCLUSION

In conclusion, we have demonstrated the first direct evidence for strong correlations in a one-dimensional system of a simple metal that leads to a possible

breakdown of FL and the emergence of TLL behavior. The value of g turns out to be very similar to semiconductor nanowires[12] and carbon nanotubes,[15] implying remarkably strong electron–electron interaction for a metallic system. From an application viewpoint, the extreme sensitivity of a Tomonaga–Luttinger liquid to disorder may set a fundamental limit for the fabrication of low-resistivity interconnects for nanoelectronics applications.

Acknowledgment. We thank Thierry Giamarchi, Alejandro Lobos, Giovanni Vignale, Leonid Glazman, and Diptiman Sen for fruitful discussions. A.G. and N.R. acknowledge funding from the Department of Science and Technology. A.G. thanks Indian Space Research Organization for financial support. U.C. thanks Council of Scientific and Industrial Research for a fellowship.

Supporting Information Available: Growth of nanowires is detailed in sections S1 and S2 and depicted pictorially in Figures S1 and S2. Device fabrication procedure using the modified lithography scheme is given in section S3. In Figure S3, R *vs* $T^{-1/2}$ in a semilog plot for a sample nanowire device shows that a variable range hopping model does not fit the data. Thickness modulations in a nanowire due to Rayleigh instability is shown in Figure S4, and the adverse effects that heating (or static charges) can have on the wires are shown in Figure S5. Details of density functional calculations can be found in section S4 and Figure S6. This material is available free of charge *via* the Internet at http://pubs.acs.org.

REFERENCES AND NOTES

1. Giamarchi, T. *Quantum Physics in One Dimension*; University Press: Oxford, 2004.
2. Deshpande, V. V.; Bockrath, M.; Glazman, L.; Yacoby, A. Electron Liquids and Solids in One Dimension. *Nature* **2010**, *464*, 209–216.
3. Giuliani, G. F.; Vignale, G. *Quantum Theory of the Electron Liquid*; University Press: Cambridge, 2005.
4. Natelson, D.; Willett, R. L.; West, K. W.; Pfeiffer, L. N. Geometry-Dependent Dephasing in Small Metallic Wires. *Phys. Rev. Lett.* **2001**, *86*, 1821–1824.
5. Senthil, T. Critical Fermi Surfaces and Non-Fermi Liquid Metals. *Phys. Rev. B* **2008**, *78*, 035103.
6. Tomonaga, S. On a Relativistically Invariant Formulation of the Quantum Theory of Wave Fields. *Prog. Theor. Phys.* **1946**, *1*, 27–42.
7. Luttinger, J. M. An Exactly Soluble Model of a Many-Fermion System. *J. Math. Phys.* **1963**, *4*, 1154–1162.
8. Hu, J.; Odom, T. W.; Lieber, C. M. Chemistry and Physics in One Dimension: Synthesis and Properties of Nanowires and Nanotubes. *Acc. Chem. Res.* **1999**, *32*, 435–445.
9. Yacoby, A.; Stormer, H. L.; Wingreen, N. S.; Pfeiffer, L. N.; Baldwin, K. W.; West, K. W. Nonuniversal Conductance Quantization in Quantum Wires. *Phys. Rev. Lett.* **1996**, *77*, 4612–4615.
10. Jompol, Y.; Ford, C. J. B.; Griffiths, J. P.; Farrer, I.; Jones, G. A. C.; Anderson, D.; Ritchie, D. A.; Silk, T. W.; Schofield, A. J. Probing Spin-Charge Separation in a Tomonaga–Luttinger Liquid. *Science* **2009**, *325*, 597–601.
11. Steinberg, H.; Barak, G.; Yacoby, A.; Pfeiffer, L. N.; West, K. N.; Halperin, B. I.; Hur, K. L. Charge Fractionalization in Quantum Wires. *Nat. Phys.* **2008**, *4*, 116–119.
12. Venkataraman, L.; Hong, Y. S.; Kim, P. Electron Transport in a Multichannel One-Dimensional Conductor: Molybdenum Selenide Nanowires. *Phys. Rev. Lett.* **2006**, *96*, 076601.
13. Yuen, J. D.; Menon, R.; Coates, N. E.; Namdas, E. B.; Cho, S.; Hannahs, S. T.; Moses, D.; Heeger, A. J. Nonlinear Transport in Semiconducting Polymers at High Carrier Densities. *Nat. Mater.* **2009**, *397*, 572–575.
14. Slot, E.; Holst, M. A.; van der Zant, H. S. J.; Zaitsev-Zotov, S. V. One-Dimensional Conduction in Charge-Density-Wave Nanowires. *Phys. Rev. Lett.* **2004**, *93*, 176602.
15. Bockrath, M.; Cobden, D. H.; Lu, J.; Rinzler, A. G.; Smalley, R. E.; Balents, L.; McEuen, P. L. Luttinger-Liquid Behaviour in Carbon Nanotubes. *Nature* **1999**, *397*, 598–601.
16. Postma, H. W. C.; Teepen, T.; Yao, Z.; Grifoni, M.; Dekker, C. Carbon Nanotube Single-Electron Transistors at Room Temperature. *Science* **2001**, *293*, 76–79.
17. Yao, Z.; Postma, H. W. C.; Balents, L.; Dekker, C. Carbon Nanotube Intramolecular Junctions. *Nature* **1999**, *402*, 273–276.
18. Blumenstein, C., Schfer, J., Mietke,S., Meyer, S., Dollinger, A., Lochner, M., Cui, X. Y., Patthey, L., Matzdorf, R.; Claessen, R. Atomically Controlled Quantum Chains Hosting a Tomonaga–Luttinger Liquid. *Nat. Phys.* Submitted for publication, Doi:10.1038/nphys205.
19. Haruyama, J.; Takesue, I.; Hasegawa, T.; Sato, Y. Coulomb Blockade Related to a Localization Effect in a Single Tunnel-Junction/Carbon-Nanotube System. *Phys. Rev. B* **2001**, *63*, 073406.
20. Peng, Y.; Cullis, T.; Inkson, B. Accurate Electrical Testing of Individual Gold Nanowires by *In-Situ* Scanning Electron Microscope Nanomanipulators. *Appl. Phys. Lett.* **2008**, *93*, 183112.
21. Kondo, Y.; Takayanagi, K. Synthesis and Characterization of Helical Multi-shell Gold Nanowires. *Science* **2000**, *289*, 606–608.
22. Rodrigues, V.; Fuhrer, T.; Ugarte, D. Signature of Atomic Structure in the Quantum Conductance of Gold Nanowires. *Phys. Rev. Lett.* **2000**, *85*, 4124–4127.
23. Huo, Z.; Tsung, C.-k.; Huang, W.; Zhang, X.; Yang, P. Sub-Two Nanometer Single Crystal Au Nanowires. *Nano Lett.* **2008**, *8*, 2041–2044.
24. Halder, A.; Ravishankar, N. Ultrafine Single-Crystalline Gold Nanowire Arrays by Oriented Attachment. *Adv. Mater.* **2007**, *19*, 1854–1858.
25. Kundu, P.; Halder, A.; Viswanath, B.; Kundu, D.; Ramanath, G.; Ravishankar, N. Nanoscale Heterostructures with Molecular-Scale Single-Crystal Metal Wires. *J. Am. Chem. Soc.* **2010**, *132*, 20–21.
26. Wang, C.; Sun, S. Facile Synthesis of Ultrathin and Single-Crystalline Au Nanowires. *Chem. Asian J.* **2009**, *4*, 1028–1034.
27. Wang, C.; Hu, Y.; Lieber, C. M.; Sun, S. Ultrathin Au Nanowires and Their Transport Properties. *J. Am. Chem. Soc.* **2008**, *130*, 8902–8903.
28. Lu, Y.; Huang, J. Y.; Wang, C.; Sun, S.; Lou, J. Cold Welding of Ultrathin Gold Nanowires. *Nat. Nanotechnol.* **2010**, *5*, 218–224.
29. Altshuler, B. L.; Aronov, A. G. In *Electron-Electron Interactions in Disordered Systems*; Efros, A. L., Pollak, M., Eds.; Elsevier: Amsterdam, 1985.
30. Rodin, A. S.; Fogler, M. M. Apparent Power-Law Behavior of Conductance in Disordered Quasi-One-Dimensional Systems. *Phys. Rev. Lett.* **2010**, *105*, 106801.
31. Schulz, H. J. Wigner Crystal in One Dimension. *Phys. Rev. Lett.* **1993**, *71*, 1864–1867.
32. Matveev, K. A.; Glazman, L. I. Coulomb Blockade of Tunneling into a Quasi-One-Dimensional Wire. *Phys. Rev. Lett.* **1993**, *70*, 990–993.
33. Sun, Y.; Mayers, B.; Xia, Y. Transformation of Silver Nanospheres into Nanobelts and Triangular Nanoplates through a Thermal Process. *Nano Lett.* **2003**, *3*, 675–679.
34. Kane, C. L.; Fisher, M. P. A. Transport in a One-Channel Luttinger Liquid. *Phys. Rev. Lett.* **1992**, *68*, 1220–1223.